

# GaussianDiffusion: 3D Gaussian Splatting for Denoising Diffusion Probabilistic Models with Structured Noise

Xinhai Li<sup>1</sup>

Harbin Institute of Technology (Shenzhen)  
Shenzhen, China

lixinhaiyk@gmail.com

Huaibin Wang<sup>2</sup>

Harbin Institute of Technology (Shenzhen)  
Shenzhen, China

22S051022@stu.hit.edu.cn

Kuo-Kun Tseng<sup>3</sup>

Harbin Institute of Technology (Shenzhen)  
Shenzhen, China

kktseng@hit.edu.cn

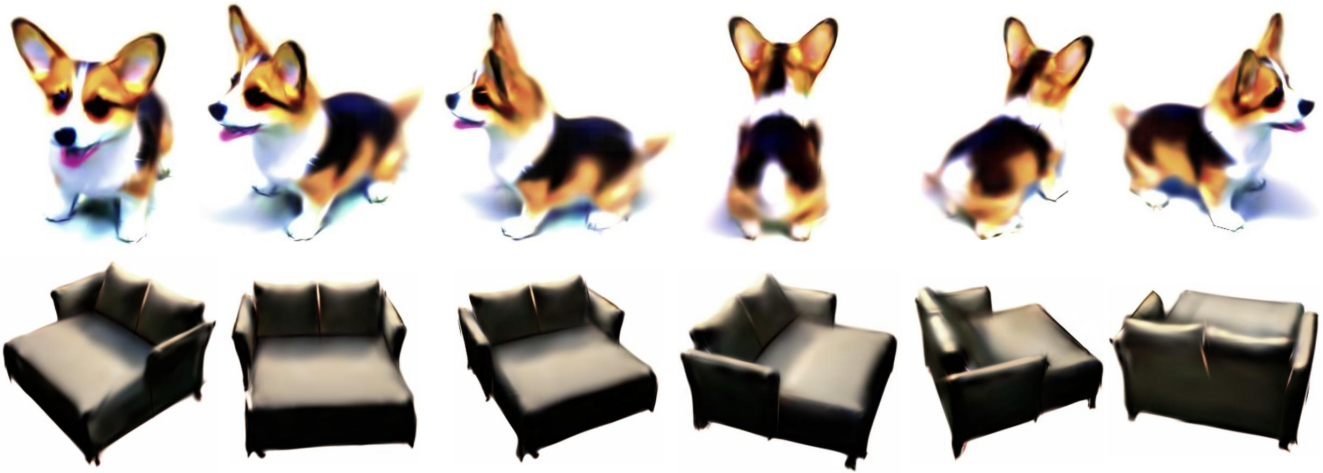


Figure 1. GaussianDiffusion text-to-3D generation, given the text prompts 'a corgi' and 'a hamburger'.

## Abstract

*Text-to-3D, known for its efficient generation methods and expansive creative potential, has garnered significant attention in the AIGC domain. However, the pixel-wise rendering of NeRF and its ray marching light sampling constrain the rendering speed, impacting its utility in downstream industrial applications. Gaussian splatting has recently shown a trend of replacing the traditional point-wise sampling technique commonly used in NeRF-based methodologies, and it is changing various aspects of 3D reconstruction. This paper introduces a novel text to 3D content generation framework based on Gaussian splatting and produces more realistic renderings. The challenge of achieving multi-view consistency in 3D generation significantly impedes modeling complexity and accu-*

*racy. Taking inspiration from SJC, we explore employing multi-view noise distributions to perturb images generated by 3D Gaussian splatting, aiming to rectify inconsistencies in multi-view geometry. We ingeniously devise an efficient method to generate noise that produces Gaussian noise from diverse viewpoints, all originating from a shared noise source. Furthermore, vanilla 3D Gaussian-based generation tends to trap models in local minima, causing artifacts like floaters, burrs, or proliferative elements. To mitigate these issues, we propose the variational Gaussian splatting technique to enhance the quality and stability of 3D appearance. To our knowledge, our approach represents the first comprehensive utilization of Gaussian splatting across the entire spectrum of 3D content generation processes.*

## 1. Introduction

3D content generation [3, 16, 18, 20, 26, 29, 35–37, 42, 43] based on large language models [7, 30] has garnered widespread attention, marking a significant advancement in modern industries such as gaming, media, interactive virtual reality, and robotics applications. Traditional 3D asset creation is a labor-intensive process that relies on well-trained designers to produce a single 3D asset, involving tasks like geometric modeling, shape baking, UV mapping, material design, and texturing. Hence, there is a pressing need for an automated approach to achieve high-quality 3D content generation with consistent geometry across multi-views and rich materials and textures.

Gaussian Splatting [11] is currently showing a trend of replacing the traditional pointwise sampling approach used in NeRF-based methodologies, leading to a paradigm shift in multiple domains of 3D reconstruction. The unique representation offered by 3D Gaussian splatting not only enables a continuous portrayal of 3D scenes but also seamlessly integrates with traditional rendering pipelines in a discreet form. Therefore, it greatly accelerates the rendering speed of 3D models in downstream applications.

DreamFusion [26] pioneered the learning of 3D contents from 2D diffusion models through score distillation sampling (SDS), and then followed these excellent text-to-3D solutions [3, 10, 15, 35, 42, 44–46, 49, 51]. SJC solves the out-of-distribution (OOD) problem between the standard normal of the 2D diffusion model input and the 3D rendering, through secondary noise addition to 3D rendering. 3DFuse [35] uses a multi-stage coarse-to-fine method to guide the direction of 3D model generation, uses view-specific depth as a condition, and applies controlNet [50] to control the direction of Diffusion model generation.

However, there are currently several challenges associated with learning 3D content from a 2D pretrained diffusion model. When using a given text prompt, the generation of multi-view 2D diffusion tends to result in multi-view geometric consistency issue. Simultaneously, the rendering speed imposes limitations on the advancement of relevant applications, particularly for NeRF-Based pointwise query and rendering methods, making it challenging to extend the 3D generation framework to practical projects. What is more, 3D content generation based on the vanilla 3D Gaussian is susceptible to the model getting trapped in local extreme points, leading to artifacts such as burrs, floaters, or proliferative elements in 3D models. Therefore, this paper focuses on using text prompts for 3D content generation and explores possibilities to overcome these limitations.

In summary, our main contributions are as follows:

- We propose a novel text-to-3D framework based on the Gaussian splatting rendering pipeline and the score function, Langevin dynamics diffusion model. GaussianDiffusion significantly speeds up the rendering process and

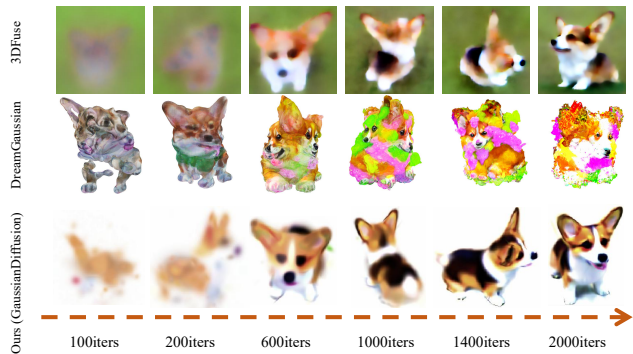


Figure 2. Comparison of convergence speed.

is able to produce the most realistic appearance currently achievable in text-to-3D tasks.

- We introduce structured noise from various viewpoints for the first time, aiming to tackle the challenge of maintaining multi-view geometric consistency, such as the problem of multi-faceted structures, through a noise injection approach. Furthermore, we propose an effective method for generating noise based on Gaussian Splatting.
- To address the inherent contradiction between precise Gaussian graphics modeling and the instability observed in 2D diffusion models across multiple views, we introduce a variational Gaussian Splatting model to mitigate the risk of the 3D Gaussian model converging to local minima, which may cause artifacts like floaters, burrs or proliferative elements.

## 2. Related Works

### 2.1. Diffusion models

Diffusion models [8, 38, 40], have recently gained widespread attention in the field of 2D image generation owing to their stability, versatility, and scalability. In the text-to-image domain, CLIP [30] was first introduced to guide text-to-image generation by GLIDE [23]. Subsequently, there have been many developments in text-to-image frameworks that offer higher resolutions and fidelity, such as Imagen [33], DALL-E2 [31], and Stable-Diffusion [32]. The emergence of numerous 2D text-to-image models has laid the groundwork for 3D generation. This allows 3D models to build upon mature 2D generation models, utilizing them as teacher models for distillation-based learning.

### 2.2. 3D Gaussian Splatting

3D Gaussian splatting [11] provides a promising and efficient approach for 3D scene representation. It employs a collection of 3D Gaussian spheres to characterize spatial scenes, with each sphere carrying information about position, scale, color, opacity, and rotation. These spheres

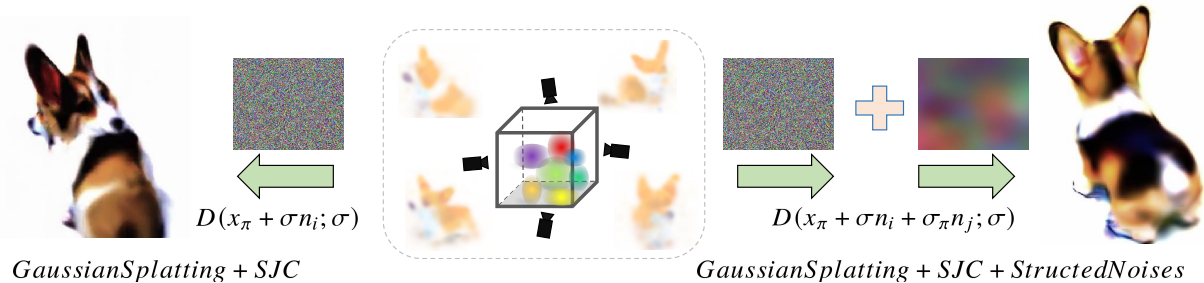


Figure 3. Structured Noise. The left portion in the figure represents the SJC method. It involves adding noise to  $x_\pi$  to gradually transform it into a standard normal distribution  $N(0, I)$ , and evaluate  $D(x_\pi + \sigma n_i; \sigma)$  through diffusion model. The right portion corresponds to our structured noise approach, which generates additional  $N(0, 1)$  distributions related to both pose and pixel position from the same noise source. This establishes inherent noise constraints between images generated from different viewpoints, addressing the multi-view consistency problem.

are projected into 2D based on camera poses and subsequently blended using  $\alpha$ -compositing according to their distances to the screen. Through differentiable rendering and gradient-based optimization, the model approximates the rendered images to match the provided ground truth. The unique representation offered by 3D Gaussian splatting not only enables a continuous portrayal of 3D scenes but also seamlessly integrates with traditional rendering pipelines in a discreet form. Thanks to its versatile representation, it has already sparked significant advancements in various directions within NeRF-based methodologies [1, 4, 12, 21, 22, 25, 27, 28, 41, 47, 48, 52].

### 2.3. Image-to-3D generation

The vast amount of image data [6, 17] available holds immense potential for single-image-to-3D content generation tasks. At the same time, the maturity of 2D diffusion models [8, 38, 40] has brought new opportunities to excellent frameworks in single-image 3D generation [2, 18, 19, 29, 36, 43]. However, generating 3D content from a single image limits the generation and imagination capabilities of computers. Therefore, adopting a text-to-3D approach aligns better with the human-computer interaction model.

### 2.4. Text-to-3D generation

Dreamfusion [26] pioneered the use of score distillation sampling (SDS) to learn 3D scenes from frozen 2D diffusion models. SJC [45] addressed the Out-of-Distribution (OOD) problem between standard normal inputs of 2D diffusion models and 3D rendered images by introducing secondary noise on 3D rendered images through a perturbation process. 3DFuse [35] serves as the baseline for our work, guiding the 3D model generation direction in multiple stages, from coarse to fine, while using view-specific depth as a condition and employing ControlNet [50] to guide the generation direction of the Diffusion model. TANGO [13]

transfers the appearance style of a given 3D shape according to a text prompt in a photorealistic manner. However, the method requires a 3D model as input. DreamGaussian [42] is our concurrent work, which is based on SDS [26], while we draw inspiration from SJC [45], and apply score function and Langevin sampling method [38] to recover structure knowledge from Gaussian noise. Our work, GaussianDiffusion, applies Gaussian splatting across the entire spectrum of 3D generation process. Latest text-to-3D works [3, 10, 15, 44, 46, 49, 51] produce realistic, multi-view consistent object geometry and color from a given text prompt, unfortunately, NeRF-based generation is time-consuming, and cannot meet industrial needs.

### 2.5. Multiface Problem

The previous methods, such as incorporating viewpoint features [14, 20, 29, 37], required fine-tuning diffusion models on Objaverse [5] data, which involved supervised training. However, due to Objaverse’s style influencing 2D diffusion models, fine-tuning tends to result in 3D appearances with an artistic style. Moreover, due to neural network forgetting, this approach severely diminishes the original 2D diffusion model’s generalization performance. On the other hand, our structured noise method, akin to SJC [45], doesn’t require fine-tuning and doesn’t alter the distribution of the original 2D diffusion model. It preserves its generalization capability and realism. Our structured noise is rendered from random Gaussian spheres, combined with the target scene, and then recovered through denoising to produce the 3D scene. This process is a form of self-supervised self-constraint training within the same distribution, shown in Figure 5, ensuring the preservation of both generalization capability and realism, making it straightforward and effective.

### 3. Method

#### 3.1. 3D Gaussian Splatting for SJC

The current state-of-the-art baseline for 3D reconstruction is the 3D Gaussian splatting [11], known for its fast rendering and the discretized representation of 3D scenes, significantly facilitating 3D generation and editing. Each Gaussian in the scene is defined by multiple parameters encapsulated in  $\theta = \{z, s, q, \alpha, c\}$ , where the position  $z \in \mathbb{R}^3$ , a scaling factor  $s \in \mathbb{R}^3$ , opacity  $\alpha \in \mathbb{R}$ , rotation quaternion  $q \in \mathbb{R}^4$ , and color feature  $c \in \mathbb{R}^3$  are considered.

Our objective is to model and sample from the distribution  $p(\theta)$ , to generate new 3D content. Let  $p_\sigma(\mathbf{x})$  denote the data distribution perturbed by Gaussian noise of standard deviation  $\sigma$ . As discussed in [2, 39], the denoising score can be approximated as follows, where  $D$  is the denoiser.

$$\nabla_x \log p_\sigma(\mathbf{x}) \approx \frac{D(\mathbf{x}; \sigma) - \mathbf{x}}{\sigma^2} \quad (1)$$

SJC [45] assumes that the probability density of 3D asset  $\theta$  is proportional to the expected probability densities of its multiview 2D image renderings  $\mathbf{x}_\pi$  over camera poses  $\pi$ :

$$p_\sigma(\theta) \propto \mathbb{E}_\pi[p_\sigma(\mathbf{x}_\pi(\theta))] \quad (2)$$

$P_\sigma(\theta)$  characterizes the 3D distribution of  $\theta$  with the inclusion of a 3D noise perturbation  $\sigma$ . On the right side of the equation, perturbing with the same 2D Gaussian distribution would inevitably result in confusion from multiple viewpoints. Thus,  $\sigma$  needs to incorporate a view-dependent condition  $\pi$ . Our motivation stems from the concept of perturbing data with noise projected from a common source across various viewpoints, rather than applying 2D noise sampled from the same distribution to generate images. Therefore, Equation 2 can be refined as:

$$p_\sigma(\theta) \propto \mathbb{E}_\pi[p_{\sigma_\pi}(\mathbf{x}_\pi(\theta))] \quad (3)$$

Where  $p_{\sigma_\pi}$  denotes the data distribution perturbed by Gaussian noise  $\sigma_\pi$  projected from a common noise source with viewpoint  $\pi$ . So the lower bound can be rewritten as:

$$\log p_\sigma(\theta) = \log[\mathbb{E}(p_{\sigma_\pi}(\mathbf{x}_\pi))] - \log Z \quad (4)$$

where  $Z = \int \mathbb{E}_\pi[p_{\sigma_\pi}(\mathbf{x}_\pi(\theta))]d\theta$  denotes the normalization constant. So according to the chain rule [45]:

$$\nabla_\theta \log \tilde{p}_\sigma(\theta) = \mathbb{E}_\pi[\nabla_\theta \log p_{\sigma_\pi}(\mathbf{x}_\pi)] \quad (5)$$

$$\frac{\partial \log \tilde{p}_\sigma(\theta)}{\partial \theta} = \mathbb{E}_\pi \left[ \frac{\partial \log p_{\sigma_\pi}(\mathbf{x}_\pi)}{\partial \mathbf{x}_\pi} \cdot \frac{\partial \mathbf{x}_\pi}{\partial \theta} \right] \quad (6)$$

$$\underbrace{\nabla_\theta \log \tilde{p}_\sigma(\theta)}_{\text{3D score}} = \mathbb{E}_\pi \left[ \underbrace{\nabla_{\mathbf{x}_\pi} \log p_{\sigma_\pi}(\mathbf{x}_\pi)}_{\text{2D score; pretrained}} \cdot \underbrace{\mathcal{J}_\pi}_{\text{renderer Jacobian}} \right]. \quad (7)$$

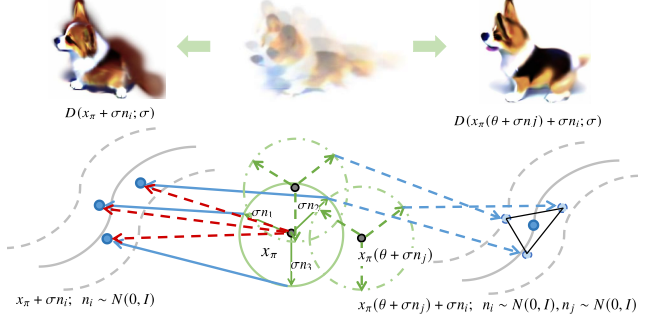


Figure 4. Variational Gaussian Splatting. The left portion is the SJC [45] method, which involves adding noise to  $x_\pi$  to gradually transform it into a standard normal distribution  $N(0, I)$ , and then evaluate  $D(x_\pi + \sigma n_i; \sigma)$  through diffusion model. On the right, leveraging the variational Gaussian splatting method involves pre-designing a Gaussian model for the parameters  $\theta$ . During the gradient backward, the gradient is propagated to the mean, while the variance retains the noise level introduced by the diffusion model. The objective is to learn a distribution that more accurately conforms to the correct parameter space by introducing slight variations within a defined range. The distribution points on the triangle are determined by jittering, and then the mean of the distribution is taken as the value for forward inference.

So, the current challenge revolves around efficiently constructing viewpoint-related noise  $\sigma_\pi$  and utilizing it to perturb  $p(x_\pi(\theta))$ , resulting in  $p_{\sigma_\pi}(x_\pi(\theta))$ .

#### 3.2. 3D Noise Generation and Projection

For the sake of ensuring positive semi-definiteness, the Gaussian Splatting method is crafted with physically meaningful covariances:

$$\Sigma = R s s^T R^T \quad (8)$$

Where  $s$  represents the scale matrix,  $R$  represents the rotation matrix. In the computation,  $s$  is used to denote the scale of a 3D vector along the three axes and a quaternion  $q$  is used to represent the rotation matrix  $R$ . Given the viewpoint transformation  $W$ ,  $J$  representing the Jacobian of the affine approximation of the projective transformation, the 2D covariance can be projected as:

$$\Sigma' = J W \Sigma W^T J^T \quad (9)$$

After projecting the 3D Gaussian ellipsoid onto a 2D plane, it is represented as a bivariate Gaussian distribution on the current ellipse. For a given pixel  $U(u_1, v_2)$ , the opacities of the Gaussian spheres contributing to that pixel from front to back are  $\alpha_1, \alpha_2, \dots, \alpha_n$ . The final opacities are calculated using Equation 10, where  $z_\pi$  is the projection of the Gaussian sphere position  $z$  onto the viewpoint  $\pi$ .

$$\alpha'_i(U) = \alpha_i * e^{-(z_\pi - U) \Sigma' (z_\pi - U)^T} \quad (10)$$

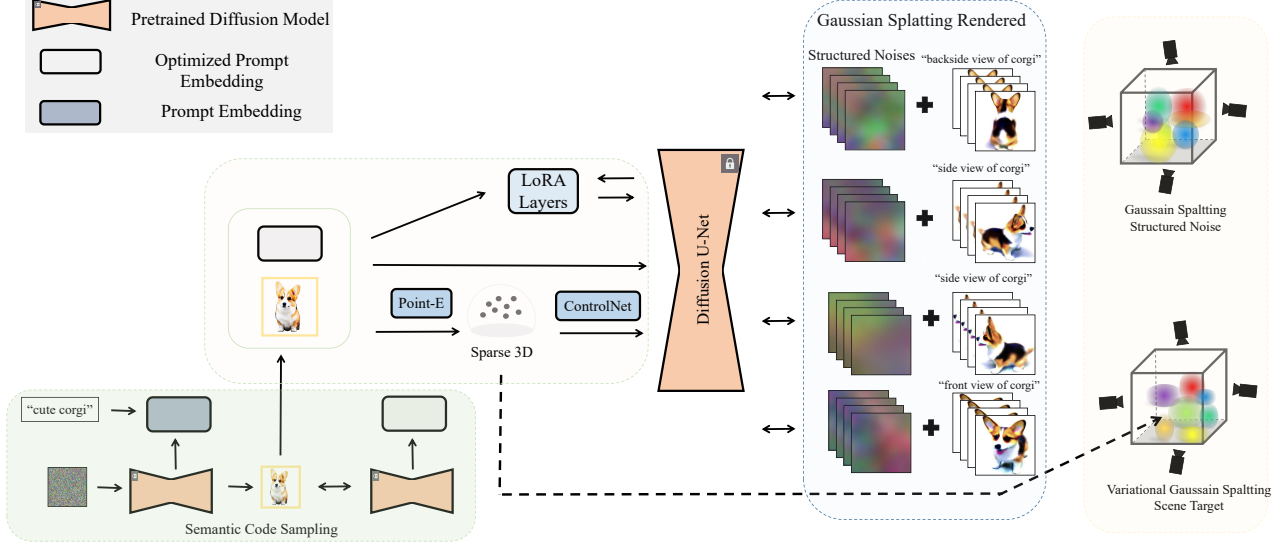


Figure 5. GaussianDiffusion Framework. We apply Semantic Code Sampling module [35] to restrict the entire 3D scene to a singular semantic identity. An optimized image, derived from Semantic Code Sampling, generates a sparse point cloud using Point-E [24]. This point cloud is subsequently pose-projected into a depth map, functioning as a constraint for ControlNet [50]. Concurrently, LoRA [9] is deployed for additional optimization for fine-tuning of the diffusion model. The sparse point cloud produced by Point-E acts as the initial input to Gaussian Splatting [11]. Leveraging SDS [26], the gradient of the diffusion model is conveyed to Gaussian Splatting. In order to address challenges related to multi-view consistency and the presence of artifacts such as floaters burrs or proliferative elements, we introduce Structured Noise and the Variational Gaussian Splatting method to produce realistic 3D appearance.

Through the  $\alpha$ -blending, the final color is then determined by:

$$\begin{aligned}
 C &= \sum_{i=1}^n \alpha'_i c_i \prod_{j=1}^{i-1} (1 - \alpha'_j) \\
 &= \alpha'_1 c_1 + (1 - \alpha'_1) \left[ \sum_{i=2}^n \alpha'_i c_i \prod_{j=2}^{i-1} (1 - \alpha'_j) \right]
 \end{aligned} \tag{11}$$

Let  $c_1, c_2, \dots, c_n$  follow a normal distribution, and the intermediate term  $\alpha'_{n-1} c_{n-1} + (1 - \alpha'_{n-1}) c_n$  also follows a normal distribution, the iterative process from back to front results in  $C$  following a normal distribution.

When the initial 3D noise positions  $z$ , are uniformly distributed within the range  $[-0.5, 0.5]$ , and they do not change over time, given pixel coordinates  $U(u_1, u_2)$ , and a fixed camera viewpoint  $\pi$ , with fixed  $W$  and  $J$ , then  $\alpha' = \alpha * e^{-(z_\pi - U)\Sigma'(z_\pi - U)^T} = \alpha'(U, W, J, z)$ , which signifies that  $\alpha'_n$  remains constant and does not change over time, effectively making it a constant. Consequently, the distribution of  $C$  follows a linear combination of multiple independent normal distributions and thus is also a normal distribution.

$$\begin{aligned}
 \mathbb{E}(C) &= \mathbb{E}\left[\sum_{i=1}^n \alpha'_i c_i \prod_{j=1}^{i-1} (1 - \alpha'_j)\right] \\
 &= \alpha'_1 * \mathbb{E}[c_1] + (1 - \alpha'_1) * \left(\mathbb{E}\left[\sum_{i=2}^n \alpha'_i c_i \prod_{j=2}^{i-1} (1 - \alpha'_j)\right]\right) \\
 &= 0 \\
 \text{Var}(C) &= \text{Var}\left[\sum_{i=1}^n \alpha'_i c_i \prod_{j=1}^{i-1} (1 - \alpha'_j)\right] \\
 &= \sum_{i=1}^n \alpha_i'^2 \prod_{j=1}^{i-1} (1 - \alpha_j')^2
 \end{aligned} \tag{12}$$

$$\tag{13}$$

So, for a given pixel position,  $C$  can be represented as a standard normal distribution. That is  $P(C|U, \pi) = N(0, \text{Var}(C))$  can be standardized to  $N(0, I)$ , allowing for noise to be added to the novel view synthesized by Gaussian Splatting. This noise is associated with the viewpoint  $\pi$  and does not affect the numerical stability of  $N(0, I)$  noises added by SJC, as shown in Figure 3

### 3.3. Variational Gaussian Splatting

There is an inherent contradiction between precise 3D Gaussian Splatting geometric modeling and the inconsistency of multiple views in 2D diffusion model. Beyond the

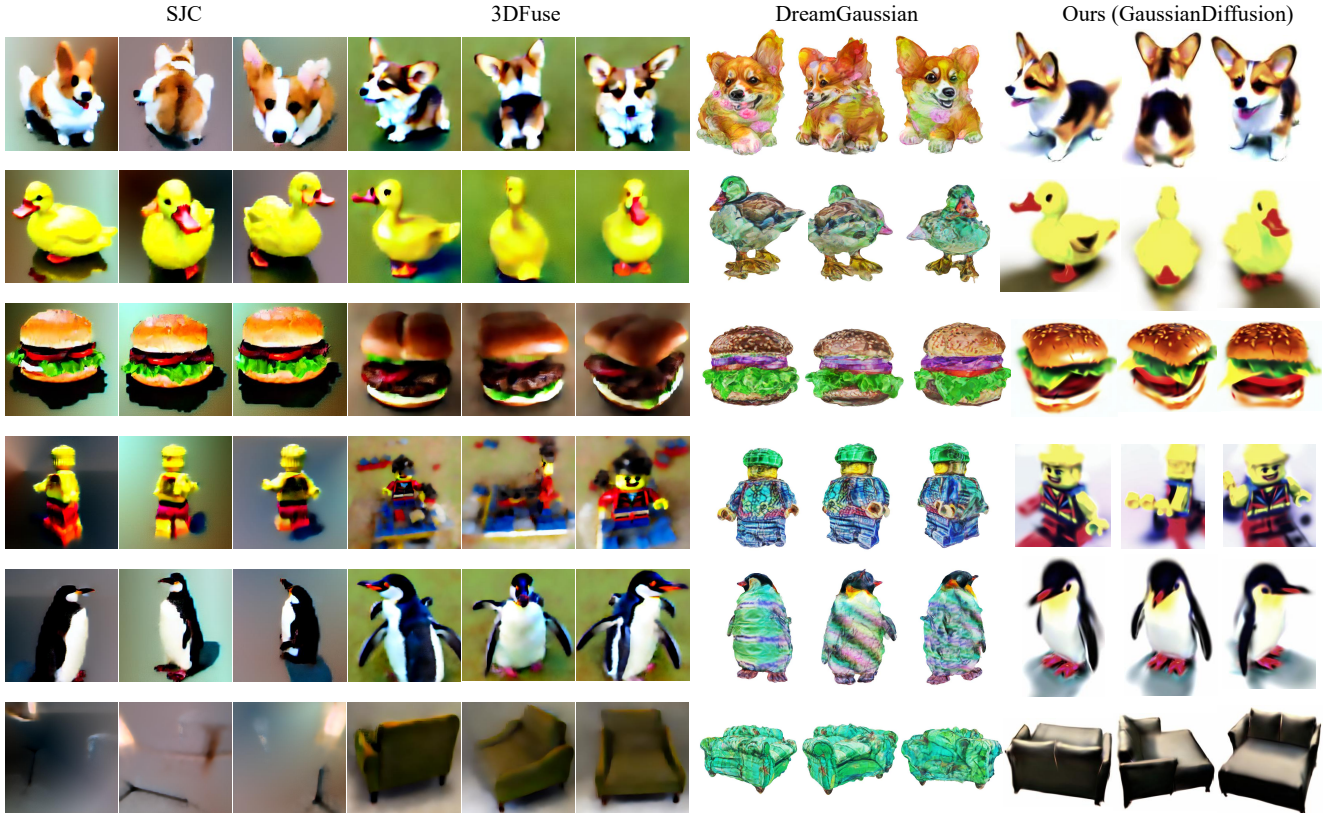


Figure 6. Comparison between SJC, 3DFuse, DreamGaussian, and our GaussianDiffusion in text-to-3D, given text prompts 'a corgi,' 'a yellow duck,' 'a hamburger,' 'a Lego figure,' 'a penguin,' and 'a sofa'.

introduction of structured noise, our objective is to fundamentally resolve the imbalance between the two. We formulate the Variational Gaussian Splatting model to propagate the gradient to the distribution of  $\theta$ , intending to learn the distribution of  $\theta$  rather than fixed values. Specifically, it perturbs position  $z$  and scale  $s$  in the original Gaussian Splatting to facilitate the learned model's transition from a blurry to a precise state and from coarse to fine details.

Modeling the distribution of  $z$  and  $s$  as a Gaussian model, with the mean of  $z$  learned by Gaussian Splatting. The variance, the range of perturbations should synchronize with the noise level in the diffusion model. As mentioned in the SMLD [38], in regions of low data density, score matching may not have enough evidence to estimate score functions accurately, due to the lack of data samples. When the noise level added by the diffusion model is high, it implies that there is less gradient information in  $X_0$ , the original picture, so at this time, more perturbations should be added to the original  $z$  and  $s$  to obtain a blurrier 3D model. When the noise level added by the diffusion model is lower, it means that there is a more effective gradient flow in  $X_0$ , so correspondingly, less noise should be added to Gaussian Splatting. Guiding the model from coarse to fine, in the rough stage, the perturbations can have looser constraints,

which can better balance the multi-view geometric consistency.

For Equation 7, variational Gaussian splatting increases the convergence domain and has the ability to escape local minima. The difference between  $p_\sigma(\theta)$  and  $p_\sigma(X)$  is that  $p_\sigma(X)$  directly expresses the distribution of  $X$  with the addition of  $\sigma$  perturbations, while in the expression of  $p_\sigma(\theta)$ , there is actually a latent variable.  $p_\sigma(g(\theta))$  represents the space given by the parameter  $\theta$ , and through the mapping of the function  $g$ , it maps  $\theta$  to the 3D space, where  $g(\theta)$  represents the 3D scene space. Perturbing  $\theta$ , the coverage domain of  $g(\theta)$  expands, and when performing distillation learning on the 2D diffusion model, it helps to escape local minima and avoid artifacts such as burrs, floaters, or proliferative elements. We design the parameters  $\theta'$  to follow a Gaussian distribution  $N(\theta, \sigma)$ , where  $\sigma$  is a variance at the same level as the noise added by the diffusion model:

$$\theta' = \theta + \sigma * \mathcal{N}(0, I) \quad (14)$$

Equation 17 indicates that the gradient with respect to  $\theta'$  is equivalent to the gradient with respect to  $\theta$ . This allows for the introduction of noise perturbation without altering the gradient flow, facilitating the transition from solving for fixed values to solving for the parameter model distribution.

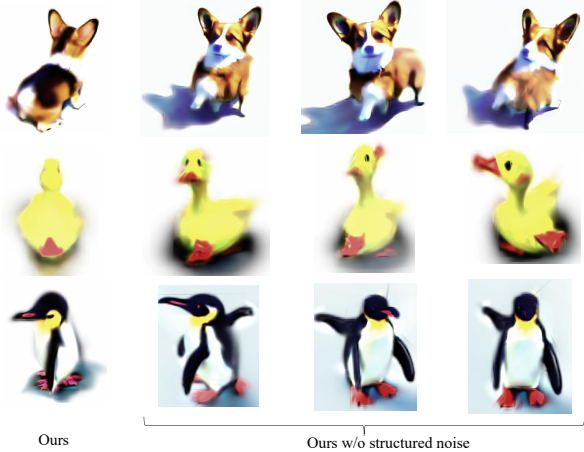


Figure 7. Ablation study. GaussianDiffusion without structured noise.

$$\frac{\partial \log \tilde{p}_\sigma(\theta)}{\partial \theta'} = \mathbb{E}_\pi \left[ \frac{\partial \log p_{\sigma_\pi}(\mathbf{x}_\pi)}{\partial \mathbf{x}_\pi} \cdot \frac{\partial \mathbf{x}_\pi}{\partial \theta'} \right] \quad (15)$$

$$= \mathbb{E}_\pi \left[ \frac{\partial \log p_{\sigma_\pi}(\mathbf{x}_\pi)}{\partial \mathbf{x}_\pi} \cdot \frac{\partial \mathbf{x}_\pi}{\partial \theta'} \cdot \frac{\partial \theta'}{\partial \theta} \right] \quad (16)$$

$$= \frac{\partial \log \tilde{p}_\sigma(\theta)}{\partial \theta} \quad (17)$$

The visualization can be seen in Figure 4. On the left, the idea of Computing PAAS [45] on 2D renderings, denoted as  $x_\pi$ , is proposed by SJC [45]. It involves adding  $\sigma n_i$  to the center  $x_\pi$  to make it approach  $\mathcal{N}(0, I)$ , addressing the out-of-distribution (OOD) problem, and then evaluate  $D(x_\pi + \sigma n_i; \sigma)$  through diffusion model. However, this may lead to the generation of artifacts in 3D Gaussian Splatting such as floaters, burrs, or proliferative elements, as illustrated on the left side of the figure. On the right, building upon this idea, we introduce perturbations to the parameter  $\theta$ , resulting in additional dashed circles after perturbing  $x_\pi$ . These circles correspond to multiple blurred corgis. Variational Gaussian splatting method involves pre-designing a Gaussian model for the parameters  $\theta$ . During the gradient backward, the gradient is propagated to the mean, while the variance retains the noise level introduced by the diffusion model. Through a more relaxed convergence constraint, we ensure that the optimization does not get stuck in a local optimum as shown in the top-left figure, but instead converges to a global optimal solution, as illustrated in the top-right figure.

## 4. Experiment

### 4.1. Overall Pipeline

As shown in Figure 5, we introduce the Semantic Code Sampling module within 3DFuse [35] to address the chal-

lenge of text prompt ambiguity. In this method, an image is initially generated using the provided text prompt, after which the prompt embedding is optimized based on the resultant image. Subsequently, we apply LoRA [9] adaptation to maintain semantic information and fine-tune the Diffusion model. To integrate 3D awareness into pre-trained 2D diffusion models, we employ Point-E [24] to generate a sparse point cloud from a single image. This point cloud is then projected to derive a depth map utilizing the specified camera pose  $\pi$ . Furthermore, we incorporate spatial conditioning controls from the depth map into the text-to-image diffusion models [50]. Simultaneously, this sparse point cloud serves as the input point cloud for Gaussian Splatting initialization.

We conduct training over 2000 steps for the overall stage, whereas 3DFuse requires 10000 steps for achieving stable results. The 3D Gaussians are initially set with 0.1 opacity and a grey color within a sphere of radius 0.5. Gaussian splatting is performed at a rendering resolution of 512. Random camera poses are sampled at a fixed radius of 1, with a y-axis FOV between 40 and 70 degrees, azimuth in the range of [-180, 180] degrees, and elevation in the range of [-45, 45] degrees. The background is rendered randomly as white. The 3D Gaussians are initialized with 4096 cloud points, derived from the output of Point-E [24]. The cloud is densified every 50 steps after 300 steps and has its opacity reset for 400 steps. This opacity reset guarantees that our final appearance remains free from oversaturation. All experiments are conducted and measured using an NVIDIA 4090 (24GB) GPU.

### 4.2. Comparison of Convergence Speed

The comparison of convergence speeds can be observed in Figure 2. The convergence speed of DreamGaussian [42] is relatively high, yet it is susceptible to overfitting in later stages, lacks a continuous optimization space, and demonstrates suboptimal multi-view geometric consistency. The 3DFuse [35] method, requiring approximately 10,000 iterations for convergence to satisfactory results, still manifests issues such as overexposure and burr artifacts. Similar to fundamental NeRF-based approaches, it also renders downstream tasks at a slower pace. In contrast, our method achieves significantly faster convergence, reaching a satisfactory state around 2,000 iterations while ensuring geometric consistency. It successfully avoids artifacts like floaters burrs or proliferative elements, resulting in the generation of the most realistic appearance. Additionally, being rooted in 3D Gaussian methods, it notably enhances rendering speed without a sudden slowdown with increasing pixels. Furthermore, downstream applications seamlessly integrate with traditional rendering pipelines.

### 4.3. Structured Noise Generation Details

We ingeniously apply Gaussian Splatting to generate random pixelwise normal distribution noises. The point cloud is initialized in spherical coordinates with radii ranging from -0.5 to 0.5. Azimuth is randomly selected between -180 and 180 degrees, and elevation between -45 and 45 degrees. The initialization color of the point cloud is sampled from a standard normal distribution. As detailed in the 3D Noise Generation and Projection section, for a given pixel  $U(u_1, u_2)$  and a specified camera pose  $\pi$ , we ensure that the added noise adheres to a standard normal distribution, preserving the numerical stability of the original image. The diffusion model’s input noise comprised a combination of structural noise and SJC [45] noise, wherein the proportion of structural noise declined gradually from 0.3 to 0.05 over a span of 2000 iterations, as shown in Figure 3.

### 4.4. Variational Gaussian Splatting

We apply noise with the same magnitude variance  $\sigma$  of the frozen diffusion model and zero mean, to perturb the parameters  $z$  and  $s$  as the description of Eq 14. Based on experimental observations, we found that applying a coefficient of 0.1 to the jitter noise variance yields better results, denoted as  $\theta' = \theta + \sigma \cdot N(0, I) \cdot \gamma$ , where  $\gamma$  equals 0.15. The comparison results between whether add perturbation  $\theta$  or not can be seen as Figure 4.

### 4.5. Quantitative Comparison

We reference the geometric consistency for 3D scene generation quantification in 3DFuse [35], which is based on COLMAP [34]. The underlying principle is that COLMAP optimizes camera poses based on the multi-view geometric consistency of the 3D surface. So, we uniformly sample 100 camera poses from the hemisphere coordinates, all facing the center of the sphere with the same radius and elevation angle. We then render 100 images using these poses and predict the poses between adjacent images using COLMAP [34]. The variance of the predicted poses is used as a measure of 3D consistency. High variance indicates inaccuracies in pose prediction, implying 3D geometric inconsistency.

In Table 1, we compared the mean variance scores of 50 generated 3D scenes. Experimental data demonstrates that our method significantly outperforms SJC [45], 3DFuse [35], and DreamGaussian [42], providing strong evidence that our approach exhibits superior geometric consistency in text-to-3D tasks.

### 4.6. Qualitative Comparison

As depicted in Figure 6, we present a comparative analysis of our experimental results, wherein all methods are meticulously fine-tuned for optimal convergence. The

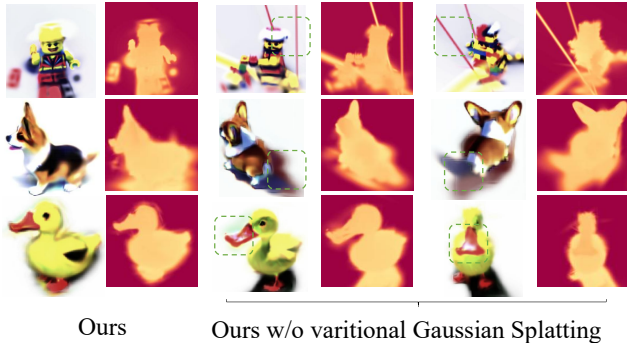


Figure 8. Ablation study. GaussianDiffusion without variational Gaussian splatting.

Method	Variance ↓	Train Iters	Training Time
SJC [45]	0.081	10000	13.8min
3DFuse [35]	0.053	10000	20.3min
DreamGaussian [42]	0.106	600	3.1min
GaussianDiffusion(Ours)	0.021	2000	5.5min

Table 1. Quantitative evaluation of mean variance in 50 generated 3D scenes based on COLMAP [34] method proposed by 3DFuse [35].

SJC [45] and 3DFuse [35] methodologies undergo training for 10,000 iterations, while DreamGaussian [42] undergoes 600 iterations, and our method is trained for 2,000 iterations. Experimental validation reveals that SJC’s earlier proposed method exhibits shortcomings in both multi-view geometric consistency and appearance. Although 3DFuse demonstrates an acceptable appearance and a certain level of geometric consistency, there are still issues with multi-view consistency, as seen in the penguin, and it contends with issues such as overexposure, floaters, burrs, or proliferative elements in appearance. DreamGaussian [42] achieves swift convergence, yet its limited subsequent optimization space and poor multi-view consistency are drawbacks. Furthermore, its texture optimization operates as a post-processing method independently of the overall pipeline. In contrast, our method, incorporating structured noises and variational Gaussian Splatting, consistently attains multi-view geometric consistency, yielding realistic and visually appealing outcomes.

### 4.7. Ablation Study

As depicted in Figure 3 and 7, after removing the technology of structured noise from multiple viewpoints, it is evident that there are issues with multi-view geometric consistency and multi-faceted structures. Additionally, the variance in the quantitative analysis shows a sharp decline, as illustrated in Table 2.

As illustrated in Figure 4 and 8, replacing the variational Gaussian Splatting technique with vanilla Gaussian Splatting results in numerous floaters, burrs, or proliferative

Method	Variance ↓	Train Iters
GaussianDiffusion w/o Structured Noise	0.056	2000
GaussianDiffusion w/o Variational Gaussian	0.033	2000
GaussianDiffusion(Ours)	0.021	2000

Table 2. Ablation study. We compared the effects after removing structured noise and variational Gaussian Splatting with the results obtained from the complete version.

elements. The quantitative analysis shows a slight decrease in variance, as indicated in Table 2.

## 5. Discussion and Conclusion

This paper introduces a 3D content generation framework based on Gaussian Splatting, significantly accelerating rendering speed while achieving the most realistic appearance to date in text-to-3D tasks. By incorporating structured noise from multiple viewpoints, we address the challenge of multi-view geometric inconsistency. What is more, the variational Gaussian Splatting technique enhances the generated appearance by mitigating artifacts like floaters, burrs proliferative elements. While the current results demonstrate improved realism compared to prior methods, the utilization of variational Gaussian introduces some degree of blurriness and haze. Consequently, our forthcoming research endeavors aim to rectify and enhance this aspect.

## References

- [1] Jonathan T Barron, Ben Mildenhall, Matthew Tancik, Peter Hedman, Ricardo Martin-Brualla, and Pratul P Srinivasan. Mip-nerf: A multiscale representation for anti-aliasing neural radiance fields. In *Proceedings of the IEEE/CVF International Conference on Computer Vision*, pages 5855–5864, 2021. 3
- [2] Eric R Chan, Connor Z Lin, Matthew A Chan, Koki Nagano, Boxiao Pan, Shalini De Mello, Orazio Gallo, Leonidas J Guibas, Jonathan Tremblay, Sameh Khamis, et al. Efficient geometry-aware 3d generative adversarial networks. In *Proceedings of the IEEE/CVF Conference on Computer Vision and Pattern Recognition*, pages 16123–16133, 2022. 3, 4
- [3] Rui Chen, Yongwei Chen, Ningxin Jiao, and Kui Jia. Fantasia3d: Disentangling geometry and appearance for high-quality text-to-3d content creation. *arXiv preprint arXiv:2303.13873*, 2023. 2, 3
- [4] Zhiqin Chen, Thomas Funkhouser, Peter Hedman, and Andrea Tagliasacchi. Mobilenerf: Exploiting the polygon rasterization pipeline for efficient neural field rendering on mobile architectures. In *Proceedings of the IEEE/CVF Conference on Computer Vision and Pattern Recognition*, pages 16569–16578, 2023. 3
- [5] Matt Deitke, Dustin Schwenk, Jordi Salvador, Luca Weihs, Oscar Michel, Eli VanderBilt, Ludwig Schmidt, Kiana Ehsani, Aniruddha Kembhavi, and Ali Farhadi. Objaverse: A universe of annotated 3d objects. In *Proceedings of the IEEE/CVF Conference on Computer Vision and Pattern Recognition*, pages 13142–13153, 2023. 3
- [6] Jia Deng, Wei Dong, Richard Socher, Li-Jia Li, Kai Li, and Li Fei-Fei. Imagenet: A large-scale hierarchical image database. In *2009 IEEE conference on computer vision and pattern recognition*, pages 248–255. Ieee, 2009. 3
- [7] Alexey Dosovitskiy, Lucas Beyer, Alexander Kolesnikov, Dirk Weissenborn, Xiaohua Zhai, Thomas Unterthiner, Mostafa Dehghani, Matthias Minderer, Georg Heigold, Sylvain Gelly, et al. An image is worth 16x16 words: Transformers for image recognition at scale. *arXiv preprint arXiv:2010.11929*, 2020. 2
- [8] Jonathan Ho, Ajay Jain, and Pieter Abbeel. Denoising diffusion probabilistic models. *Advances in neural information processing systems*, 33:6840–6851, 2020. 2, 3
- [9] Edward J Hu, Yelong Shen, Phillip Wallis, Zeyuan Allen-Zhu, Yuanzhi Li, Shean Wang, Lu Wang, and Weizhu Chen. Lora: Low-rank adaptation of large language models. *arXiv preprint arXiv:2106.09685*, 2021. 5, 7
- [10] Yukun Huang, Jianan Wang, Yukai Shi, Xianbiao Qi, Zheng-Jun Zha, and Lei Zhang. Dreamtime: An improved optimization strategy for text-to-3d content creation. *arXiv preprint arXiv:2306.12422*, 2023. 2, 3
- [11] Bernhard Kerbl, Georgios Kopanas, Thomas Leimkühler, and George Drettakis. 3d gaussian splatting for real-time radiance field rendering. *ACM Transactions on Graphics (TOG)*, 42(4):1–14, 2023. 2, 4, 5
- [12] Xin Kong, Shikun Liu, Marwan Taher, and Andrew J Davison. vmap: Vectorised object mapping for neural field slam. In *Proceedings of the IEEE/CVF Conference on Computer Vision and Pattern Recognition*, pages 952–961, 2023. 3
- [13] Jiabao Lei, Yabin Zhang, Kui Jia, et al. Tango: Text-driven photorealistic and robust 3d stylization via lighting decomposition. *Advances in Neural Information Processing Systems*, 35:30923–30936, 2022. 3
- [14] Weiyu Li, Rui Chen, Xuelin Chen, and Ping Tan. Sweetdreamer: Aligning geometric priors in 2d diffusion for consistent text-to-3d. *arXiv preprint arXiv:2310.02596*, 2023. 3
- [15] Yuhan Li, Yishun Dou, Yue Shi, Yu Lei, Xuanhong Chen, Yi Zhang, Peng Zhou, and Bingbing Ni. Focaldreamer: Text-driven 3d editing via focal-fusion assembly. *arXiv preprint arXiv:2308.10608*, 2023. 2, 3
- [16] Chen-Hsuan Lin, Jun Gao, Luming Tang, Towaki Takikawa, Xiaohui Zeng, Xun Huang, Karsten Kreis, Sanja Fidler, Ming-Yu Liu, and Tsung-Yi Lin. Magic3d: High-resolution text-to-3d content creation. In *Proceedings of the IEEE/CVF Conference on Computer Vision and Pattern Recognition*, pages 300–309, 2023. 2
- [17] Tsung-Yi Lin, Michael Maire, Serge Belongie, James Hays, Pietro Perona, Deva Ramanan, Piotr Dollár, and C Lawrence Zitnick. Microsoft coco: Common objects in context. In *Computer Vision—ECCV 2014: 13th European Conference, Zurich, Switzerland, September 6–12, 2014, Proceedings, Part V 13*, pages 740–755. Springer, 2014. 3
- [18] Minghua Liu, Chao Xu, Haiyan Jin, Linghao Chen, Zexiang Xu, Hao Su, et al. One-2-3-45: Any single image to 3d mesh

- in 45 seconds without per-shape optimization. *arXiv preprint arXiv:2306.16928*, 2023. 2, 3
- [19] Ruoshi Liu, Rundi Wu, Basile Van Hoorick, Pavel Tokmakov, Sergey Zakharov, and Carl Vondrick. Zero-1-to-3: Zero-shot one image to 3d object. In *Proceedings of the IEEE/CVF International Conference on Computer Vision*, pages 9298–9309, 2023. 3
- [20] Yuan Liu, Cheng Lin, Zijiao Zeng, Xiaoxiao Long, Lingjie Liu, Taku Komura, and Wenping Wang. Syncdreamer: Generating multiview-consistent images from a single-view image. *arXiv preprint arXiv:2309.03453*, 2023. 2, 3
- [21] Ben Mildenhall, Pratul P Srinivasan, Matthew Tancik, Jonathan T Barron, Ravi Ramamoorthi, and Ren Ng. Nerf: Representing scenes as neural radiance fields for view synthesis. *Communications of the ACM*, 65(1):99–106, 2021. 3
- [22] Thomas Müller, Alex Evans, Christoph Schied, and Alexander Keller. Instant neural graphics primitives with a multiresolution hash encoding. *ACM Transactions on Graphics (ToG)*, 41(4):1–15, 2022. 3
- [23] Alex Nichol, Prafulla Dhariwal, Aditya Ramesh, Pranav Shyam, Pamela Mishkin, Bob McGrew, Ilya Sutskever, and Mark Chen. Glide: Towards photorealistic image generation and editing with text-guided diffusion models. *arXiv preprint arXiv:2112.10741*, 2021. 2
- [24] Alex Nichol, Heewoo Jun, Prafulla Dhariwal, Pamela Mishkin, and Mark Chen. Point-e: A system for generating 3d point clouds from complex prompts. *arXiv preprint arXiv:2212.08751*, 2022. 5, 7
- [25] Sida Peng, Yuanqing Zhang, Yinghao Xu, Qianqian Wang, Qing Shuai, Hujun Bao, and Xiaowei Zhou. Neural body: Implicit neural representations with structured latent codes for novel view synthesis of dynamic humans. In *Proceedings of the IEEE/CVF Conference on Computer Vision and Pattern Recognition*, pages 9054–9063, 2021. 3
- [26] Ben Poole, Ajay Jain, Jonathan T Barron, and Ben Mildenhall. Dreamfusion: Text-to-3d using 2d diffusion. *arXiv preprint arXiv:2209.14988*, 2022. 2, 3, 5
- [27] Sergey Prokudin, Michael J Black, and Javier Romero. Smpix: Neural avatars from 3d human models. In *Proceedings of the IEEE/CVF Winter Conference on Applications of Computer Vision*, pages 1810–1819, 2021. 3
- [28] Albert Pumarola, Enric Corona, Gerard Pons-Moll, and Francesc Moreno-Noguer. D-nerf: Neural radiance fields for dynamic scenes. In *Proceedings of the IEEE/CVF Conference on Computer Vision and Pattern Recognition*, pages 10318–10327, 2021. 3
- [29] Guocheng Qian, Jinjie Mai, Abdullah Hamdi, Jian Ren, Aliaksandr Siarohin, Bing Li, Hsin-Ying Lee, Ivan Skokhodov, Peter Wonka, Sergey Tulyakov, et al. Magic123: One image to high-quality 3d object generation using both 2d and 3d diffusion priors. *arXiv preprint arXiv:2306.17843*, 2023. 2, 3
- [30] Alec Radford, Jong Wook Kim, Chris Hallacy, Aditya Ramesh, Gabriel Goh, Sandhini Agarwal, Girish Sastry, Amanda Askell, Pamela Mishkin, Jack Clark, et al. Learning transferable visual models from natural language supervision. In *International conference on machine learning*, pages 8748–8763. PMLR, 2021. 2
- [31] Aditya Ramesh, Prafulla Dhariwal, Alex Nichol, Casey Chu, and Mark Chen. Hierarchical text-conditional image generation with clip latents. *arXiv preprint arXiv:2204.06125*, 2022. 2
- [32] Robin Rombach, Andreas Blattmann, Dominik Lorenz, Patrick Esser, and Björn Ommer. High-resolution image synthesis with latent diffusion models. In *Proceedings of the IEEE/CVF conference on computer vision and pattern recognition*, pages 10684–10695, 2022. 2
- [33] Chitwan Saharia, William Chan, Saurabh Saxena, Lala Li, Jay Whang, Emily L Denton, Kamyar Ghasemipour, Raphael Gontijo Lopes, Burcu Karagol Ayan, Tim Salimans, et al. Photorealistic text-to-image diffusion models with deep language understanding. *Advances in Neural Information Processing Systems*, 35:36479–36494, 2022. 2
- [34] Johannes L Schonberger and Jan-Michael Frahm. Structure-from-motion revisited. In *Proceedings of the IEEE conference on computer vision and pattern recognition*, pages 4104–4113, 2016. 8
- [35] Junyoung Seo, Wooseok Jang, Min-Seop Kwak, Jaehoon Ko, Hyeonsu Kim, Junho Kim, Jin-Hwa Kim, Jiyoung Lee, and Seungryong Kim. Let 2d diffusion model know 3d-consistency for robust text-to-3d generation. *arXiv preprint arXiv:2303.07937*, 2023. 2, 3, 5, 7, 8
- [36] Ruoxi Shi, Hansheng Chen, Zhuoyang Zhang, Minghua Liu, Chao Xu, Xinyue Wei, Linghao Chen, Chong Zeng, and Hao Su. Zero123++: a single image to consistent multi-view diffusion base model. *arXiv preprint arXiv:2310.15110*, 2023. 3
- [37] Yichun Shi, Peng Wang, Jianglong Ye, Mai Long, Kejie Li, and Xiao Yang. Mvdream: Multi-view diffusion for 3d generation. *arXiv preprint arXiv:2308.16512*, 2023. 2, 3
- [38] Yang Song and Stefano Ermon. Generative modeling by estimating gradients of the data distribution. *Advances in neural information processing systems*, 32, 2019. 2, 3, 6
- [39] Yang Song and Stefano Ermon. Improved techniques for training score-based generative models. *Advances in neural information processing systems*, 33:12438–12448, 2020. 4
- [40] Yang Song, Jascha Sohl-Dickstein, Diederik P Kingma, Abhishek Kumar, Stefano Ermon, and Ben Poole. Score-based generative modeling through stochastic differential equations. *arXiv preprint arXiv:2011.13456*, 2020. 2, 3
- [41] Edgar Sucar, Shikun Liu, Joseph Ortiz, and Andrew J Davison. imap: Implicit mapping and positioning in real-time. In *Proceedings of the IEEE/CVF International Conference on Computer Vision*, pages 6229–6238, 2021. 3
- [42] Jiaxiang Tang, Jiawei Ren, Hang Zhou, Ziwei Liu, and Gang Zeng. Dreamgaussian: Generative gaussian splatting for efficient 3d content creation. *arXiv preprint arXiv:2309.16653*, 2023. 2, 3, 7, 8
- [43] Junshu Tang, Tengfei Wang, Bo Zhang, Ting Zhang, Ran Yi, Lizhuang Ma, and Dong Chen. Make-it-3d: High-fidelity 3d creation from a single image with diffusion prior. *arXiv preprint arXiv:2303.14184*, 2023. 2, 3

- [44] Christina Tsalicoglou, Fabian Manhardt, Alessio Tonioni, Michael Niemeyer, and Federico Tombari. Textmesh: Generation of realistic 3d meshes from text prompts. *arXiv preprint arXiv:2304.12439*, 2023. 2, 3
- [45] Haochen Wang, Xiaodan Du, Jiahao Li, Raymond A Yeh, and Greg Shakhnarovich. Score jacobian chaining: Lifting pretrained 2d diffusion models for 3d generation. In *Proceedings of the IEEE/CVF Conference on Computer Vision and Pattern Recognition*, pages 12619–12629, 2023. 3, 4, 7, 8
- [46] Zhengyi Wang, Cheng Lu, Yikai Wang, Fan Bao, Chongxuan Li, Hang Su, and Jun Zhu. Prolificdreamer: High-fidelity and diverse text-to-3d generation with variational score distillation. *arXiv preprint arXiv:2305.16213*, 2023. 2, 3
- [47] Alex Yu, Ruilong Li, Matthew Tancik, Hao Li, Ren Ng, and Angjoo Kanazawa. Plenotrees for real-time rendering of neural radiance fields. In *Proceedings of the IEEE/CVF International Conference on Computer Vision*, pages 5752–5761, 2021. 3
- [48] Alex Yu, Vickie Ye, Matthew Tancik, and Angjoo Kanazawa. pixelnerf: Neural radiance fields from one or few images. In *Proceedings of the IEEE/CVF Conference on Computer Vision and Pattern Recognition*, pages 4578–4587, 2021. 3
- [49] Chaohui Yu, Qiang Zhou, Jingliang Li, Zhe Zhang, Zhibin Wang, and Fan Wang. Points-to-3d: Bridging the gap between sparse points and shape-controllable text-to-3d generation. In *Proceedings of the 31st ACM International Conference on Multimedia*, pages 6841–6850, 2023. 2, 3
- [50] Lvmin Zhang, Anyi Rao, and Maneesh Agrawala. Adding conditional control to text-to-image diffusion models. In *Proceedings of the IEEE/CVF International Conference on Computer Vision*, pages 3836–3847, 2023. 2, 3, 5, 7
- [51] Joseph Zhu and Peiye Zhuang. Hifa: High-fidelity text-to-3d with advanced diffusion guidance. *arXiv preprint arXiv:2305.18766*, 2023. 2, 3
- [52] Zihan Zhu, Songyou Peng, Viktor Larsson, Weiwei Xu, Hujun Bao, Zhaopeng Cui, Martin R Oswald, and Marc Pollefeys. Nice-slam: Neural implicit scalable encoding for slam. In *Proceedings of the IEEE/CVF Conference on Computer Vision and Pattern Recognition*, pages 12786–12796, 2022. 3